RSC Applied Interfaces

ROYAL SOCIETY OF CHEMISTRY

PAPER

View Article Online
View Journal | View Issue

Cite this: *RSC Appl. Interfaces*, 2025, **2**, 210

Silicon oxide nanofibers using fungi mycelium as template material/from water purification to space insulation†

Björn K. Birdsong,*[a] Antonio J. Capezza,[a] Maryam Nejati,[b] Anton Bjurström,[ac] Yuanyuan Li,[a] Amparo Jiménez-Quero*[bd] and Richard T. Olsson*[a]

Mycelium derived from Ganoderma lucidum was employed as a template for synthesising silicon oxide (SiO_x) nanofibers. The intricate structures of mycelial hyphae fibrils were replicated with high precision using an inexpensive commercial silane (3-aminopropyl)-triethoxysilane (APTES). Following the removal of the organic mycelium template phase at 600 °C, APTES was successfully converted to SiO_x. The resulting SiO_x fibres retained the morphology of the mycelium template, with a nearly identical fibre density to the original fibrous network. A fibril diameter reduction of approximately 43% was observed from 603 to 344 nm. All synthesised materials exhibited coherent structural integrity, sufficient for handling without breakage, although they were notably less mechanically flexible than the original mycelium template. The novel hybrid mycelium-3-aminopropyl-silsesquioxane fibre network and the thermally converted SiO_x network displayed notable liquid absorption properties. These materials allowed for the preferential absorption of oil or water, depending on the presence of the amino group functionality. Remarkably, the SiO_x network rapidly absorbed methylene blue-dyed water within 400 ms, demonstrating behaviour opposite to the virgin mycelium network. Additionally, the materials exhibited high thermal stability, withstanding flame exposure at approximately 1400 °C while maintaining their nano/micromorphology. This innovative approach of using "living" templates expands the range of morphologies that can be replicated in inorganic materials, enabling the creation of genetically and environmentally tuneable structures. The SiO_x nanofibers produced through this method have potential applications in various fields, including water purification, biosensors, catalytic support, and insulation.

Received 10th September 2024,
Accepted 10th November 2024

DOI: 10.1039/d4lf00314d

rsc.li/RSCApplInter

Introduction

Materials derived from fungi are gaining popularity as potentially ground-breaking building materials due to their ease of shaping and sustainability, particularly the ability to use food waste as a growth medium.[1–3] Mycelia, the vegetative part of fungi consists of a network of hyphae, filaments capable of growing in nearly any direction and configuration, these fibrous networks serve various functions, including nutrient uptake, gas exchange, and the production of secondary metabolite.[4] To fulfil this role, fungi have evolved to grow thin, long, and relatively uniform 1–2 micrometre thick filaments, similar to many plastic fibres but with the added advantage of being naturally grown. This unique characteristic makes them ideal for a wide range of applications, including their use as a template material.[5,6]

One appealing trait of fungi for templating is the ability to manipulate the nutrient-acquiring behaviour of mycelium to influence its growth morphology, enabling the creation of customisable fibrous templates. Additionally, the structural morphology of the mycelium can be further controlled by selecting specific fungi species and drying methods, allowing for the formation of templating fibres ranging from a few microns to several meters in length.[6] This unique characteristic makes them ideal for a wide range of applications such as biomedical scaffolds, bio-composites, acoustic and thermal insulation, including their use as a template material for replicating the fibrous network morphology into a secondary material.[7,8] Here, thin silicon oxide structures sharing a similar morphology as mycelium

[a] *Department of Fiber and Polymer Technology, School of Chemical Science and Engineering, KTH Royal Institute of Technology, SE-100 44 Stockholm, Sweden. E-mail: birdsong@kth.se, rols@kth.se*
[b] *Division of Glycoscience, Department of Chemistry, School of Engineering Sciences in Chemistry, Biotechnology and Health, Royal Institute of Technology, SE-106 91, Stockholm, Sweden*
[c] *NKT HV Cables, Technology Consulting, SE-721 78, Västerås, Sweden*
[d] *Division of Industrial Biotechnology, Department of Life Sciences, Chalmers University of Technology, 412 96 Gothenburg, Sweden. E-mail: amparo@chalmers.se*

† Electronic supplementary information (ESI) available. See DOI: https://doi.org/10.1039/d4lf00314d

can be imagined for numerous applications ranging from water purification, biosensors, catalytic support, and insulation due to their chemical, mechanical, and thermal stability.[9–12] As a precursor to silicon oxide, a silane (silsesquioxane precursor) can be used as an inexpensive and industrially widely used surface treatment chemical to replicate fibrous biomaterials. The silsesquioxane precursors are used in a wide variety of applications ranging from coupling agents to precursors of silicon materials. An essential factor for being the most used precursor is its ability to convert from silane into silanol *via* either acidic or alkaline conditions.[13–15] In this more reactive state, silanol can condense with hydroxyl groups found on the surface of a wide range of materials, from cellulose to metals.[16] The downside of this reactivity is that silanol often forms various by-products by self-condensation in the form of amorphous Si–O–Si structures, which limits its use in the finest and most uniform coatings.[17,18] Some silanes, such as (3-aminopropyl)triethoxysilane (APTES), are less prone to self-condensation due to their stereochemistry, resulting in a silane able to be used for coating applications with minimal formation of byproducts.[19–21] By adjusting the reaction speed of the silanol condensation, it is possible to form thin and very even coating layers on various substrates, allowing for finely detailed morphology to be replicated.[22] These coatings are chemically resistant due to the strong Si–O–Si bonds formed during the condensation reaction and also thermally stable, making it possible to remove the coated structure using chemical or thermal means from nanoparticle surfaces.[23]

In this work, the replication of the mycelia hyphae morphology was investigated using (3-aminopropyl)-triethoxysilane (APTES), resulting in a silicon oxide material that closely replicated the original mycelium hyphae material. Energy-dispersive X-ray spectroscopy (EDS) and scanning electron microscopy (SEM) were used to verify the composition of the produced materials and the accuracy of the templating method in mimicking the mycelium hyphae. Furthermore, to investigate the structure of the silane coating on the mycelium hyphae, Fourier transform infrared spectroscopy (FTIR), and X-ray diffraction (XRD) were used to demonstrate that the formed silicon oxide material was amorphous and had formed covalent bonds to the surface of the mycelium.

Experimental

Mycelium cultivation and preparation of organic template

Mycelial material was produced by cultivating *Ganoderma lucidum* strain M9725 (Mycelia, Belgium) on a potato dextrose agar (PDA) substrate. Following an incubation period of 5 days at a temperature of 30 °C, fragments measuring 1 × 1 cm from the resultant mycelia were used to inoculate a sterile potato dextrose broth medium. The inoculated medium was then incubated at 25 °C for 12 days. Lastly, to conclude the cultivation process, the exopolysaccharide gel-like structure found at the interface of the fungi and the growth medium was removed by scraping, and the remaining material was freeze-dried to remove water and for further use.

Silicon oxide replication of mycelium hyphae structure

The synthesis of APTES-coated mycelium and silicon oxide nanofibers was done using the method depicted in Fig. 1. First, mycelium material was coated using (3-aminopropyl) triethoxysilane (APTES) by immersing 73 mg of the previously produced mycelia in a solution composed of 8.520 mL propanol and 1.880 mL MQw, followed by the addition of 0.786 mL (low), 1.572 mL (medium), or 3.144 mL (high) APTES. The solutions were then left on a shake table for 24 hours to initiate the condensation of the APTES. After which, 0.260 mL ammonia hydroxide (28%) was added and allowed to react for 24 hours.

The coated mycelium materials were then washed three times using 98% ethanol and once using MQw, after which the materials were frozen using liquid nitrogen and dried using a HyperCOOL (HCC-3110, Republic of Korea) freeze drier with a pressure <0.1 mbar. To remove the mycelium hyphae template, the coated materials were placed in a high-temperature oven (T + M M9-1200) at (T = 586 °C, 2 h, 1 atm), after which the samples were stored in polypropylene tubes until further analysis.

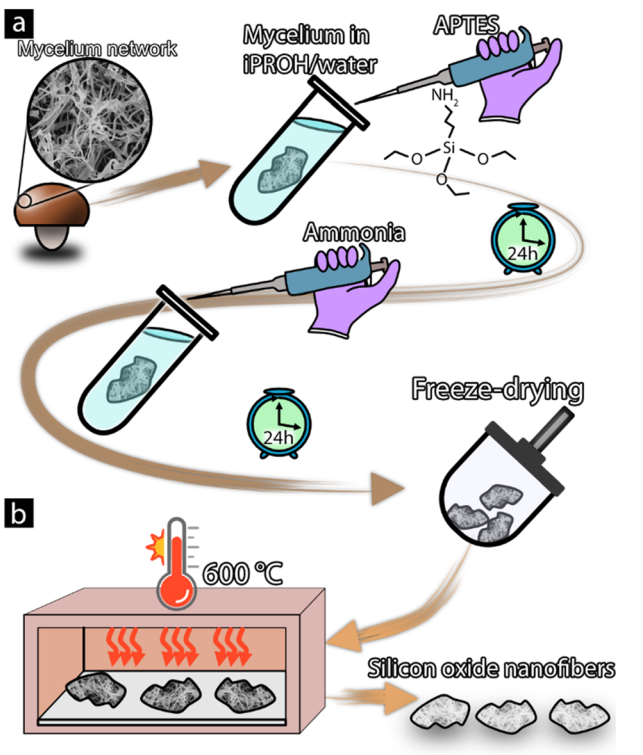

Fig. 1 Illustration of silicon oxide nanofibers, APTES coating reaction (a), liquid and template removal (b).

Characterisation

Liquid absorption capacity evaluation

The material's ability to absorb water, oil, or a mixture of both was investigated using a Dino-Light handheld digital microscope (AM4517MT-FUW, Netherlands) with DinoXcope software. The materials were recorded during the instance that the samples came into contact with the liquid phase. After *ca.* 3 min of contact with the liquid, the materials were filmed again to observe liquid retention. To determine the amount of oil and water absorbed, the samples were soaked in an equal volume part mixture for 1 min and weighed, then placed in an oven at 110 °C for 3 h and weighed again.

Fourier transform infrared spectroscopy (FTIR)

Fourier transform infrared spectroscopy (FTIR) was measured on the freeze-dried materials (mycelium, APTES-coated mycelium, heat-treated APTES-coated mycelium), using a PerkinElmer Spectrum 100, equipped with an ATR accessory, MIR TGS detector, and Specac Golden gate with a sapphire crystal. Measurements were performed using 16 consecutive scans within the range of 600 to 4000 cm^{-1}, a scanning rate of 1 cm^{-1}, and a resolution of 4 cm^{-1}.

Microstructure characterisation

The structure and morphology of the coated mycelium materials were investigated using a field emission scanning electron microscope (FE-SEM; Hitachi S-4800, Japan). The samples were placed on conductive carbon tape, and images were taken at an accelerated voltage between 1–3 kV and a current of 10 μA. The dimensions of the materials were determined by averaging 50 measured randomly selected fibres for each sample using ImageJ®, National Institutes of Health, Bethesda, Maryland, USA.

Energy-dispersive X-ray spectroscopy (EDS)

To determine the relative elemental abundance in the materials, a field emission scanning electron microscope (FE-SEM; Hitachi S-4800, Japan) was used as an electron beam source using an accelerated voltage of 20 kV. The samples were mounted on conductive carbon tape, and three separate representative areas were selected for the data collection.

X-ray diffraction (XRD)

To determine any potential crystalline structures present in the coated mycelium materials, XRD was investigated using a PANalytical X'pert PRO X-ray diffractometer

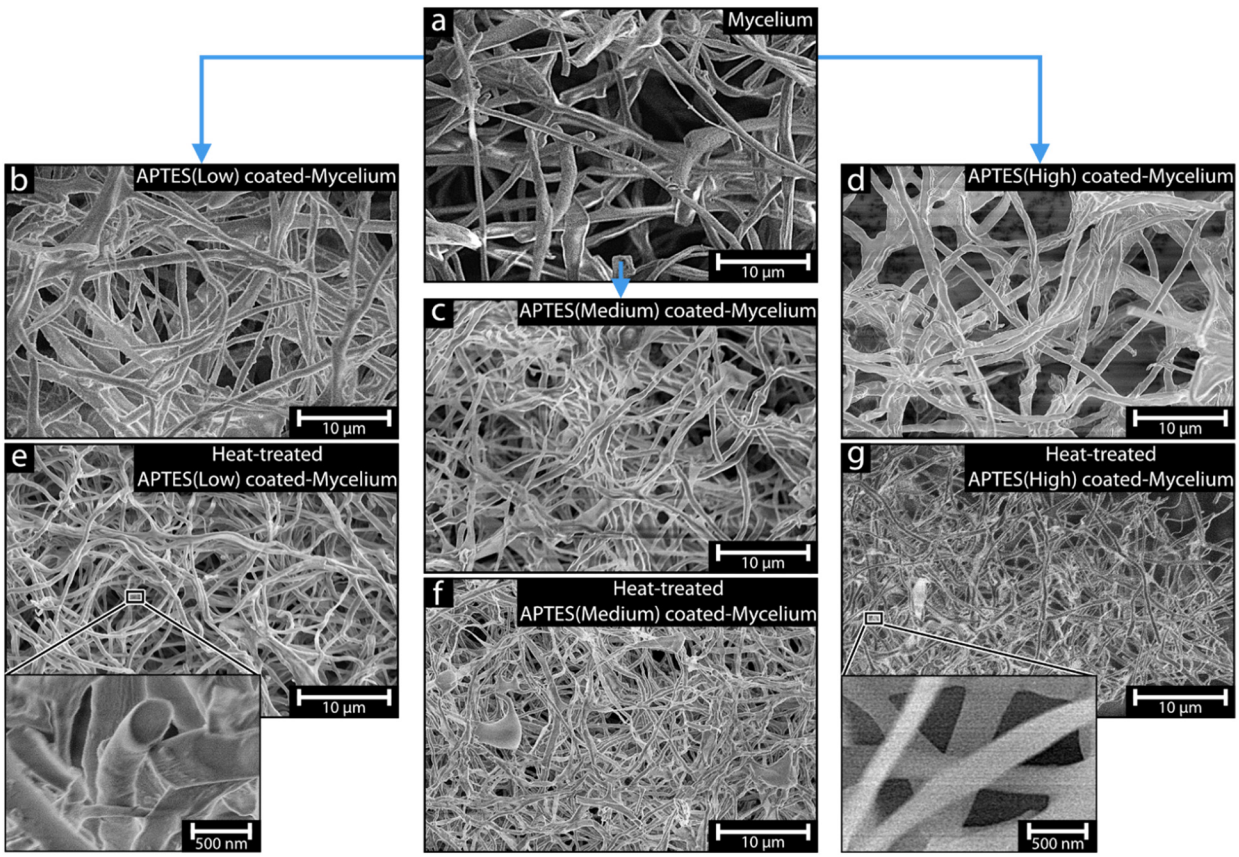

Fig. 2 Scanning electron microscope (SEM) images of the mycelium template (a), APTES-coated mycelium low, medium, and high (b–d), and the *ca.* 600 °C heat-treated APTES-coated mycelium low, medium, and high (e–g).

equipped with a Cu Kα-radiation source with a voltage and current of 45 kV and 40 mA. Measurements were performed using a step size of 0.05° between 5° to 80° and a wavelength of 0.154 nm.

Results and discussion

Microstructure of mycelium-derived materials

Fig. 2a shows the SEM micrograph depicting the mycelium template as a fibrous mat of mycelium hyphae grown in random directions of varying fibrillar thicknesses. The hyphae fibres can be seen as either individual fibres reaching tens of micrometres in length or hyphae combining *via* twisting, forming larger fibre bundles. The APTES-coated mycelium (Fig. 2b–d, low, medium, and high, respectively) show almost identical fibres compared to the pure mycelium template, with virtually no observable morphological differences.

Comparing the APTES-coated mycelium fibres diameters to the pure mycelium template fibres, it was evident that there was a slight increase in fibre thickness from the *ca.* 600 ± 180 nm thick mycelium template fibres to *ca.* 750–840 nm after the coating reactions. However, the difference in thickness between the low, medium, and high APTES coatings, representing the different concentrations used for the coating reactions, was within the measurement deviations (*ca.* 830 ± 270, 750 ± 200, and 840 ± 260 nm, respectively). The results further suggested that a maximum coating thickness was reached using even the lowest amount of APTES (see Table 1 for all fibre thicknesses).[23,24]

After the heat treatment of the APTES-coated mycelium, the morphology and structure remained virtually identical to before the heat treatment, except for a decrease in fibre thickness to *ca.* 300–400 nm, see Fig. 2e–g and Table 1. The change in thickness was suggested to be due to the removal of the mycelium template core fibre, resulting in shrinkage and possibly also involving some mineralisation reactions leading to the formation of SiO_xC_x (a denser material in comparison).[25,26] The uniformity of the fibre thickness, regardless of the APTES amount used in the coating reaction, supported the APTES ability to self-limit during the coating reaction.[24] Most importantly, no signs of an increase in fractured or broken fibres were observed for the heat-treated APTES-coated mycelium (Fig. 2e–g), suggesting that the mechanical stability of the individual fibres did not decrease in comparison to the pure mycelium and the APTES coating must have been very evenly distributed along the fibres. It is thus suggested that the brittle nature of silicon oxide was not observed due to the formation of a surprisingly uniform and thin APTES coating that was thin enough to remain flexible.[27,28]

Fig. 3a–h shows the various stages of the mycelium materials from the virgin mycelium template (Fig. 3a), the APTES-coated mycelium coated with different concentrations of APTES (Fig. 3b–d, low, medium, and high concentration, respectively), to the heat-treated APTES-coated mycelium (Fig. 3e–g), while being mechanically bent. The mycelium template (Fig. 3a), while visually identically to the APTES-coated mycelium, exhibited notable softness and flexibility, enabling considerable deformation without permanent deformation or damage to the material. In comparison, with the introduction of the APTES coating (regardless of the amount of APTES used), the material exhibited an increased stiffness and was more prone to tearing or cracking. However, the APTES-coated mycelium was flexible to handle with ease, and it allowed to be deformed sufficiently to be folded without permanent damage. In contrast, after exposure to *ca.* 600 °C for 2 h, the heat-treated APTES-coated mycelium was considerably more brittle in comparison to before heat treatment,

Table 1 Average thickness of mycelium, coated mycelium, and heat-treated coated mycelium. Values were obtained from 50 measurements on randomly selected fibres for each sample

Average fibre thickness (nm)	
Mycelium	603 ± 184
APTES (low)-mycelium	831 ± 271
APTES (medium)-mycelium	751 ± 203
APTES (high)-mycelium	835 ± 261
Heat-treated APTES (low)-mycelium	332 ± 75
Heat-treated APTES (medium)-mycelium	304 ± 125
Heat-treated APTES (high)-mycelium	397 ± 127

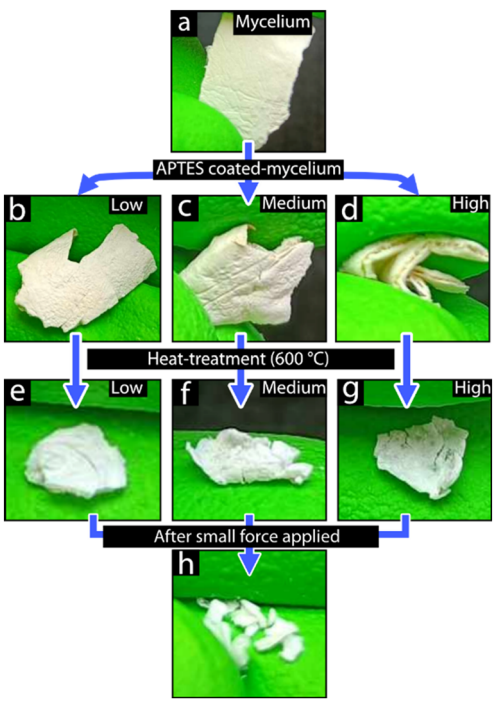

Fig. 3 Photographs of mycelium template (a), coated mycelium template material using low, medium, and high amounts of APTES (b–d), heat-treated coated mycelium using low, medium, and high amounts of APTES (e–g), and the material after a small amount of force was applied (h).

breaking apart from even slight deformation, thus requiring careful handling to not reduce the materials into smaller particles, as seen in Fig. 2h. After heat treatment, the material was slightly more translucent compared to before heat treatment, which was attributed to the removal of the carbon template material as well as the refractive index of silicon oxide being closer to that of air.[29] To further investigate and compare the surface morphology and composition of the mycelium, APTES-coated mycelium, and heat-treated APTES-coated mycelium, SEM and XRD were used.

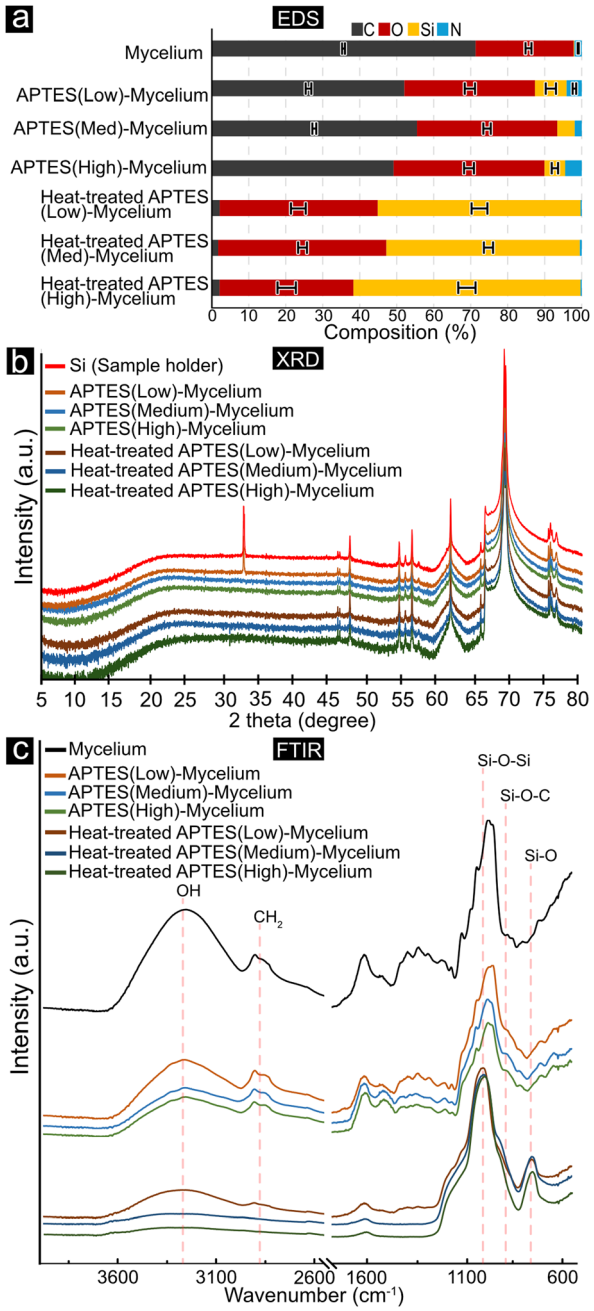

Fig. 4 illustrates the results from EDS (a), XRD (b), and FTIR (c).

Composition APTES coated-mycelium

Fig. 4 summarises the elemental composition of the materials obtained from EDS measurements (a), the X-ray diffractogram (XRD), and infrared absorption (FTIR spectra) (b and c, respectively). Fig. 4a shows that the virgin mycelium material was mainly composed of carbon and oxygen with trace amounts of nitrogen present. The composition of the virgin mycelium remained similar after the coating reactions, only shifting slightly with the introduction of the APTES coating, *i.e.*, with the presence of silicon in the material. When comparing the effect of using different concentrations of the SiO_x precursor (silane), the low, medium, and high contents in deriving the APTES-coated materials, Fig. 4a shows only minor differences in the elemental composition (<10%), suggesting that there was no significant difference in the amount of APTES on the surface of the mycelium regardless of the concentrations used. After heat treatment, the elemental composition of the materials changed to display almost purely silicon and oxygen, with only trace amounts of carbon and nitrogen left. The result demonstrates that the heat treatment at *ca.* 600 °C was adequate for the removal of the mycelium template, allowing the carbon phase to be sublimated to CO_x. Furthermore, the same ratio of silicon and oxygen was observed in all heat-treated materials, supporting the argument that the amount of APTES used did not alter the elemental composition of the final material.

The XRD patterns shown in Fig. 4b reveal that none of the materials, irrespective of the amount of APTES coating used, exhibited any detectable peaks other than the characteristic peaks of the silicon sample holder. The absence of distinct peaks, along with the presence of a broad amorphous halo, suggests that the material is predominantly amorphous, lacking any crystalline regions.[30,31] After exposure to approximately 600 °C, the XRD patterns remained unchanged, indicating that the silicon oxide material retained its amorphous nature and did not undergo any crystallisation or structural reordering during the heat treatment.

Fig. 4c shows the FTIR spectra of the template mycelium, APTES-coated mycelium, and the heat-treated APTES-coated mycelium (SiO_x). Comparing the spectra reveals that there were several key differences. The first was a decrease in the broad peak around 3400 cm^{-1} attributed to OH-vibrations, most observable when comparing the APTES-coated mycelium and the silicon oxide materials, demonstrating a more substantial decrease in relative OH in the materials upon the high-temperature exposure.[32] Second, the peaks between 2950–2870 cm^{-1}, attributed to CH_2 stretching, were almost entirely absent in the heat-treated coated mycelium spectra, further supporting the EDS results that the silicon oxide materials comprised only of silicon and oxygen.[33] Comparing the spectra of the virgin mycelium template and the APTES-coated mycelium template, there was an additional peak visible at *ca.* 920 to 950 cm^{-1}, which was

attributed to various Si–O–C bond vibrations, indicating that there was APTES present and bonded onto the mycelium material.[34] The same Si–O–C bonds were absent from the heat-treated materials, further supporting that all carbon material was removed during the heat treatment. Lastly, the heat-treated materials only show a couple of significant peaks, with the largest found at *ca.* 1030 cm^{-1} attributed to Si-O-Si and the emergence of a new peak seen at *ca.* 800 cm^{-1} attributed to Si-O vibrations, indicating that after the thermal removal of the mycelium template, the remaining material was solely comprised of an amorphous silicon oxide network.[33,35] Although the pure mycelium showed a similar peak at *ca.* 1025 cm^{-1} also found in the silicon oxide materials, the peak was attributed to C–O–C, C–O, and C–C bond stretching (found in polysaccharides) typical to mycelium.[36,37]

Liquid absorption behaviour of mycelium and mycelium-derived materials

Fig. 5a–c shows mycelium, APTES-coated mycelium, and heat-treated APTES-coated mycelium upon immediate contact with MilliQ (MQ) water dyed with methylene blue. There was an apparent difference in water absorption behaviour between the different materials. The pure mycelium material showed no visible water uptake in the fibrous material. Instead, the sugar agar portion (remaining from mycelium growth) slowly absorbed the MQ water as a wet surface formed on the sample. After the APTES modification, the APTES-coated mycelium was able to slowly absorb water inside the fibrous material. In contrast, the heat-treated APTES-coated mycelium (Fig. 2c) demonstrated an entirely different water absorption capacity than the APTES-coated mycelium and pure mycelium. In less than 400 milliseconds (see ESI† Video S1), water travelled over half the material sample length (*ca.* 5 mm). The high water uptake rate for the heat-treated APTES coated-mycelium was attributed to a combination of hydrophilicity and capillary effects from the nanoscale silicon oxide fibres.[38,39] The lack of this rapid water uptake for the APTES-coated fibrils was ascribed to the $(CH_2)_3$ group found in APTES coating before the heat treatment, which delayed the water uptake in the coated mycelium material.[40] Fig. 5d–f shows the mycelium, APTES-coated mycelium, and heat-treated APTES-coated mycelium exposed to mineral oil (see ESI Video S2). Here, in contrast to when the materials were exposed to water, all the materials showed similar behaviour, and the oil was steadily absorbed into the materials at approximately the same rate.

Fig. 5g–i shows the absorption behaviour of the materials when exposed to a mixture of oil and methylene blue-dyed water (see ESI† Video S3). The oil and dyed water emulsion were obtained by vortex mixing the mixture for 3 min and immediately exposing the materials to the emulsion before separation occurred. The pure mycelium material (Fig. 5g) showed a preference for oil absorption, which was determined by weighing measurements revealing that *ca.* 85 wt% (Fig. 5j) of the absorbed liquid was oil, further indicated by the lack of blue colour. Similarly, the APTES-coated mycelium showed the same preference for oil absorption, where the same 85 wt% (Fig. 5j) of absorbed liquid was comprised of oil. However, the APTES-coated mycelium absorbed slightly less liquid compared to the virgin mycelium. In comparison, the heat-treated APTES-coated mycelium showed more blue colouration in the absorbed liquid phase yet was less vibrant compared to the dyed water, indicating that the material was somewhat amphiphilic, which was further demonstrated when the absorbed liquid had slightly higher water content with *ca.* 82 wt% oil (Fig. 5j

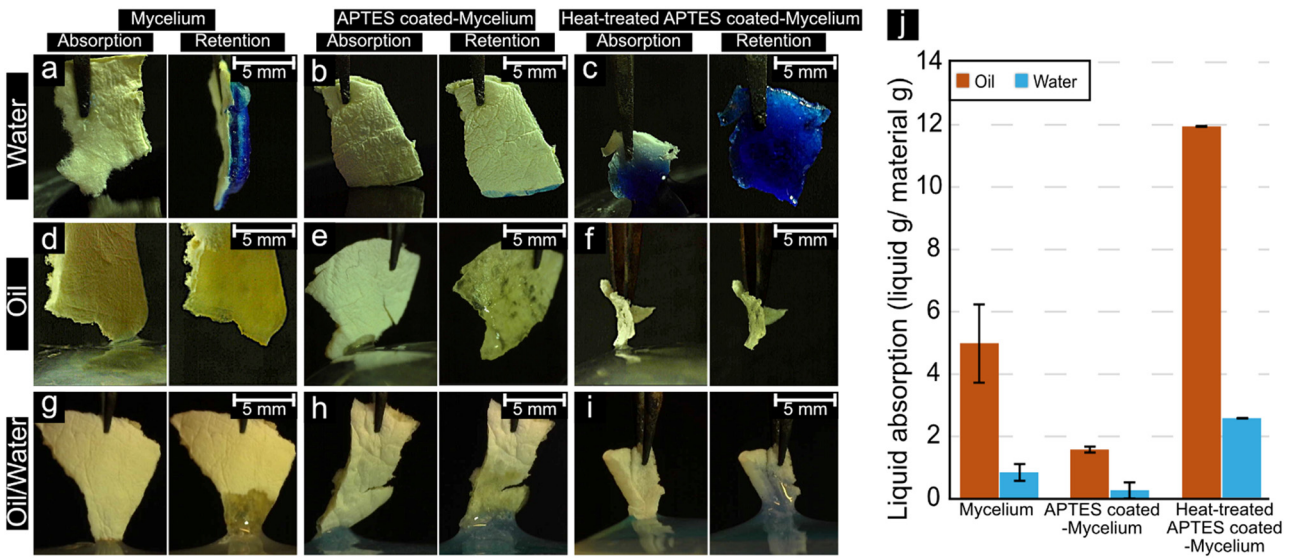

Fig. 5 Photographs of mycelium, APTES-coated mycelium, and heat-treated APTES-coated mycelium exposed to water (a–c), oil (d–f), and equal parts oil and water (g–i). The amount of liquid absorbed by mycelium, APTES (high)-coated mycelium and heat-treated APTES (high)-coated mycelium (j).

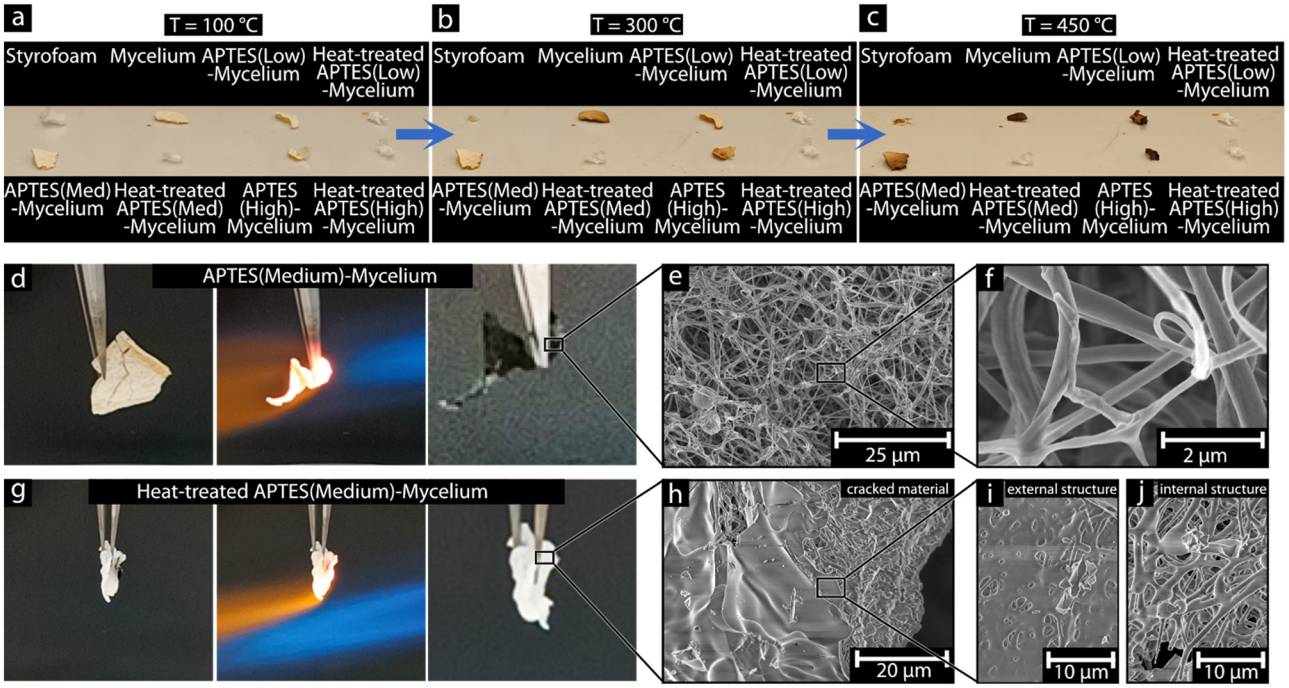

Fig. 6 Shows the effect of applied heat on Styrofoam, pure mycelium, and coated mycelium before and after removal of the mycelium template (a–c). The effect of exposure to *ca.* 1400 °C using a butane torch on APTES (medium)-mycelium and the heat-treated APTES (medium)-mycelium (d and g), and obtained SEM images of the microstructures after the high-temperature exposure of APTES (medium)-mycelium (e and f) and the heat-treated APTES (medium)-mycelium (h–j).

).[41] Although other mycelium-based materials can exhibit much higher oil selectivity, the heat-treated APTES coated-mycelium exhibited a high sorption capacity, *ca.* 12 g g^{-1} compared to 5.3 g g^{-1}, while also being thermally stable due to the silica composition.[42] The combination of selectivity, sorption capacity, and thermal stability allows heat-treated APTES coated-mycelium to be envisioned for wastewater treatment processes such as oil–water separation under harsh conditions where organic derived mycelium materials would be destroyed.[42,43]

Heat and fire behaviour of mycelium-derived silica oxide materials

Fig. 6a–c shows the effect of increased temperature on commercial Styrofoam (expanded polystyrene), the pure mycelium, the APTES-coated mycelium (low, medium, and high), and the SiO_x material after the heat-treatment of the APTES-coated mycelium (low, medium, and high), (see ESI† Video S4). All the materials exhibited stability at low temperatures (*ca.* 100 °C), showing no indication of thermal decomposition such as brown discolouration or deformation. The Styrofoam and the heat-treated APTES-coated mycelium materials all showed a strictly pure white colour, while the materials that contained the mycelium had a slight beige colouration. When the temperature was increased to *ca.* 200 °C, the Styrofoam began to deform, and the structure collapsed, while the other materials remained visually unchanged until *ca.* 300 °C was reached (Fig. 6b). At this temperature, the pure mycelium and the APTES-coated mycelium began to darken in colour, whereas the Styrofoam was reduced to a dark melt.

Overall, all the materials that contained carbon darkened and began to deform between *ca.* 350–450 °C, starting with the Styrofoam and the pure mycelium, closely followed by the APTES-coated mycelium (low, medium, and high). The darkening in colour observed for the mycelium materials corresponds to the onset of thermal decomposition, which is also seen in mycelium insulation materials and mycelium composite materials.[44] In contrast, the heat-treated APTES-coated mycelium (low, medium, and high) remained intact with no visible changes. Finally, when *ca.* 500 °C was reached (see ESI† Video S4), all that remained of the Styrofoam was char residue, while the pure mycelium had continued to deform and was heavily charred. In comparison, the APTES-coated mycelium materials had deformed somewhat and darkened, yet remained noticeably lighter in colour compared to the untreated mycelium. In contrast, the heat-treated APTES-coated mycelium materials remained unchanged in shape and colour throughout the heating range due to the highly thermally stable silicon oxide material composition.[45]

To test the limit of the material's thermal stability, the pure mycelium, APTES-coated mycelium, and heat-treated APTES-coated mycelium were subjected to over 1400 °C, using a butane torch for *ca.* 5–10 seconds, see Fig. 6d and g (see ESI† Video S5). Whereas the pure mycelium material was destroyed by the intense heat, resulting in no solid remaining

material after the exposure (see supplementary video 5), the APTES-coated mycelium, although deformed and completely blackened, remained relatively unchanged and only showed warping in its orientation, possibly caused by the force of the torch flame itself (Fig. 6d). Similarly, the heat-treated APTES-coated mycelium remained completely unchanged with only some bending observed in smaller areas, see Fig. 6g (see ESI† Video S5). The high-temperature exposed materials were further investigated using SEM imaging, Fig. 6e, f and h–j. The APTES-coated mycelium (Fig. 6e and f) and heat-treated APTES-coated mycelium (Fig. 6h–j) revealed that although the heat-treated APTES-coated mycelium appeared unchanged on the macroscopic scale, the exposure to *ca.* 1400 °C had melted and fused some of the silicon oxide fibres into a more solid shell, as can be seen in Fig. 6h and i. Despite the fused silicon oxide shell, the internal structure could be observed through cracks in the material and it showed that the silicon oxide fibres remained with small deformation due to softening and melting occurring under the melt-formed shell, Fig. 6h–j.[26] Interestingly, the APTES-coated mycelium, which was observed twisting during the high-temperature exposure (Fig. 6d), remained virtually unchanged after the 1400 °C exposure (Fig. 6e and f). The material, although black in appearance, also remained fibrous with little evidence of any morphological change. The remarkable thermo-mechanical stability was attributed to the remaining mycelium core inside the fibres, which, although charred during the heating and was trapped, as can be seen from the black colour, provided a carbon source that possibly diffused and prevented early fusion of the fibres, or reacted with the SiO_x, resulting in stiffness to the fibres, preventing softening deformation.[46] Despite the pristine fibres that could be seen in Fig. 6e and f, it was apparent that there was a limited amount of time that the organic material could survive, and all carbon was removed due to combustion at *ca.* 600 °C as previously demonstrated see Fig. 4a (EDS).

Conclusions

Materials derived from fungi are gaining popularity as potentially ground-breaking building materials due to their ease of shaping and sustainability aspects, particularly the ability to use food waste as a growth medium. This investigation into using mycelium as a template for silicon oxide fibre synthesis revealed the potential to replicate the finest filament structures of the mycelium, leading to the creation of unique silicon oxide structures previously unreported. The coating of the mycelium fibrils with APTES produced a material highly similar to the original mycelium fibre thickness. This structural integrity of the fibres was maintained after the mycelium template was removed *via* thermal treatment at around 600 °C. However, removing the mycelium template reduced mechanical flexibility, resulting in a more brittle material prone to fracturing under slight bending forces, *i.e.*, compared to the original mycelium, the mechanical properties of materials before and after removal of mycelium template could be investigated in future work to develop better understanding of the role of mycelium on the stiffness and brittleness of the materials. EDS together FTIR spectroscopy revealed the formation of C–O–Si bonds between APTES and mycelium, which, upon thermal treatment, transformed into Si–O–Si and Si–OH materials with only trace amounts of carbon remaining in the silicon oxide material. The XRD analysis confirmed the amorphous nature of the silicon oxide material, which remained unaltered even after removing the mycelium template at *ca.* 600 °C. In summary, this study shows the viability of using mycelium as a template for synthesising amorphous silicon oxide fibre structures, demonstrating formerly living organisms as precision templates for inorganic material preparation. It is suggested that the results represent a significant advance in the templating field, enabling the creation of more complex and customised templates, possibly through genetic and environmental manipulation of the growing template prior to its replication. Future studies on "living" templates should focus on exploring and comparing various fungi strains, and refining their growth patterns, to further develop the materials.[37,47] The heat-treated APTES coated-mycelium share both microscopic structures and chemical composition as the insulative materials used as heat-resistant panels for re-entry rockets, with the only exception being that the produced fibres were thinner in diameter, suggesting that the materials could potentially be used in similar applications.[12] The results herein further suggest that the materials may also be used as insulation in high-temperature applications that require thermal and mechanical stability in temperatures above 90–100 °C, where conventional Styrofoam failed to maintain its structural dimensions. The materials also hold potential for applications in biosensors, catalytic support, and wastewater treatment, owing to their adaptable properties and sustainability.[9–12] This work represents a pioneering step in using tuneable living organisms as templates for the fabrication of nanostructures, pushing the boundaries of organic/inorganic hybrid materials and paving the way for future innovations in material science.[47]

Data availability

Data will be made available on reasonable request.

Author contributions

B. K. B. performed all laboratory work included in this study. M. N. cultivated the mycelium materials used in experiments. B. K. B. performed all characterisation. B. K. B. wrote the manuscript. A. J. C., A. J.-Q., A. B., Y. Y., and R. T. O. reviewed the manuscript, with A. J. C. recognising the concept of using mycelium as a template material.

Conflicts of interest

There are no conflicts to declare.

Acknowledgements

The authors would like to acknowledge the financial contributions from the Swedish Research Council (VR 2019-05650), and the technical assistance of Dr. Xiong Xiao for XRD. A. J. C.'s contribution was funded by BioRESorb. M. N. and A. J. Q.'s contributions were funded by the Swedish Research Council Formas (Project MYCOMYM 2022-00401) and the Carl Tryggers Foundation (Project CTS 22:2169). A. B.'s contribution was supported by the Wallenberg Initiative Materials Science for Sustainability (WISE), funded by the Knut and Alice Wallenberg Foundation.

Notes and references

1 D. Lingam, S. Narayan, K. Mamun and D. Charan, Engineered mycelium-based composite materials: Comprehensive study of various properties and applications, *Constr. Build. Mater.*, 2023, **391**, 131841, DOI: **10.1016/j.conbuildmat.2023.131841**.

2 R. Abhijith, A. Ashok and C. R. Rejeesh, Sustainable packaging applications from mycelium to substitute polystyrene: a review, *Mater. Today: Proc.*, 2018, **5**, 2139–2145, DOI: **10.1016/j.matpr.2017.09.211**.

3 H.-J. Chae and J.-H. Ahn, Optimization of rice bran and food waste compost contents in mushroom culture medium to maximize mycelial growth rate and fruit body yield of Pleurotus ostreatus, *Int. Biodeterior. Biodegrad.*, 2013, **80**, 66–70, DOI: **10.1016/j.ibiod.2012.05.002**.

4 D. Moore, G. Robson and A. Trinci, *21st Century Guidebook to Fungi*, 2000.

5 A. Livne, *et al.*, A fungal mycelium templates the growth of aragonite needles, *J. Mater. Chem. B*, 2019, **7**, 5725–5731, DOI: **10.1039/C9TB01169B**.

6 M. R. Islam, G. Tudryn, R. Bucinell, L. Schadler and R. C. Picu, Morphology and mechanics of fungal mycelium, *Sci. Rep.*, 2017, **7**, 13070, DOI: **10.1038/s41598-017-13295-2**.

7 M. E. Antinori, *et al.*, Advanced mycelium materials as potential self-growing biomedical scaffolds, *Sci. Rep.*, 2021, **11**, 12630, DOI: **10.1038/s41598-021-91572-x**.

8 N. Attias, *et al.*, Mycelium bio-composites in industrial design and architecture: Comparative review and experimental analysis, *J. Cleaner Prod.*, 2020, **246**, 119037, DOI: **10.1016/j.jclepro.2019.119037**.

9 H. Mohamed Abdal-Salam Yehia and S. Mahmoud Said, Silica Nanoparticles for Water Purification and Monitoring in Point-of-Use Water Supply Systems, *Am. J. Water Resour.*, 2023, **11**, 98–102, DOI: **10.12691/ajwr-11-3-2**.

10 P. Singh, S. Srivastava, P. Chakrabarti and S. K. Singh, Nanosilica based electrochemical biosensor: A novel approach for the detection of platelet-derived microparticles, *Sens. Actuators, B*, 2017, **240**, 322–329, DOI: **10.1016/j.snb.2016.08.136**.

11 C. C. Chong, *et al.* Development of nanosilica-based catalyst for syngas production via CO2 reforming of CH4: A review, *Int. J. Hydrogen Energy*, 2021, **46**, 24687–24708, DOI: **10.1016/j.ijhydene.2020.01.086**.

12 B. Clyne, I. O. Golosnoy, J.-C. Tan and A. Markaki, Porous Materials for Thermal Management Under Extreme Conditions, *Philos. Trans. R. Soc. A.*, 2005, **364**, 125–146, DOI: **10.1098/rsta.2005.1682**.

13 K. H. J. Buschow, *Handbook of Magentic Materials*, Elsevier Amsterdam, Amsterdam, 2001, pp. 7574–7577.

14 K. H. J. Buschow, *Encyclopedia of Materials: Science and Technology*, Elsevier, 2001, pp. 1–14.

15 J. W. Morgan and E. Anders, Chemical composition of Earth, Venus, and Mercury, *Proc. Natl. Acad. Sci. U. S. A.*, 1980, **77**, 6973–6977, DOI: **10.1073/pnas.77.12.6973**.

16 S. Oyola-Reynoso, *et al.*, Revisiting the Challenges in Fabricating Uniform Coatings with Polyfunctional Molecules on High Surface Energy Materials, *Coatings*, 2015, **5**, 1002–1018.

17 K. Dhali, F. Daver, P. Cass and B. Adhikari, Surface modification of the cellulose nanocrystals through vinyl silane grafting, *Int. J. Biol. Macromol.*, 2022, **200**, 397–408, DOI: **10.1016/j.ijbiomac.2022.01.079**.

18 S. Al-Saadi and R. K. Singh Raman, Silane Coatings for Corrosion and Microbiologically Influenced Corrosion Resistance of Mild Steel: A Review, *Materials*, 2022, **15**, 1–36.

19 V. C. Karade, *et al.*, APTES monolayer coverage on self-assembled magnetic nanospheres for controlled release of anticancer drug Nintedanib, *Sci. Rep.*, 2021, **11**, 5674, DOI: **10.1038/s41598-021-84770-0**.

20 A. Zarinwall, *et al.*, Comprehensive Characterization of APTES Surface Modifications of Hydrous Boehmite Nanoparticles, *Langmuir*, 2021, **37**, 171–179, DOI: **10.1021/acs.langmuir.0c02682**.

21 R. Gadhave, C. Gadhave and P. Dhawale, Silane Terminated Prepolymers: An Alternative to Silicones and Polyurethanes, *Open J. Polym. Chem.*, 2021, **11**, 31–54, DOI: **10.4236/ojpchem.2021.113003**.

22 S. Guha Thakurta and A. Subramanian, Fabrication of dense, uniform aminosilane monolayers: A platform for protein or ligand immobilization, *Colloids Surf., A*, 2012, **414**, 384–392, DOI: **10.1016/j.colsurfa.2012.08.049**.

23 B. K. Birdsong, *et al.* Large-scale synthesis of 2D-silica (SiOx) nanosheets using graphene oxide (GO) as a template material, *Nanoscale*, 2023, **15**, 13037–13048, DOI: **10.1039/D3NR01048A**.

24 A. Mahtabani, *et al.*, Gas Phase Modification of Silica Nanoparticles in a Fluidized Bed: Tailored Deposition of Aminopropylsiloxane, *Langmuir*, 2021, **37**, 4481–4492, DOI: **10.1021/acs.langmuir.0c03647**.

25 S. Gurung, F. Gucci, G. Cairns, I. Chianella and G. J. T. Leighton, Hollow Silica Nano and Micro Spheres with Polystyrene Templating: A Mini-Review, *Materials*, 2022, **15**, 1–33, DOI: **10.3390/ma15238578**.

26 T. Rouxel, G. Massouras and G.-D. Sorarù, High Temperature Behavior of a Gel-Derived SiOC Glass: Elasticity and Viscosity, *J. Sol-Gel Sci. Technol.*, 1999, **14**, 87–94, DOI: **10.1023/A:1008779915809**.

27 G. Macrelli, A. K. Varshneya and J. C. Mauro, Ultra-thin glass as a substrate for flexible photonics, *Opt. Mater.*, 2020, **106**, 109994, DOI: **10.1016/j.optmat.2020.109994**.
28 A. P. Garcia, N. Pugno and M. J. Buehler, Superductile, Wavy Silica Nanostructures Inspired by Diatom Algae, *Adv. Eng. Mater.*, 2011, **13**, B405–B414, DOI: **10.1002/adem.201080113**.
29 G. M. Pajonk, Transparent silica aerogels, *J. Non-Cryst. Solids*, 1998, **225**, 307–314, DOI: **10.1016/S0022-3093(98)00131-8**.
30 A. Paiva, E. Guzi de Moraes, N. P. Stochero and A. Oliveira, Characterization of Vitrocrystalline Foams Produced from Discarded Glasses and Recycled Polystyrene Spheres, *Mater. Res.*, 2017, **20**, 472–478, DOI: **10.1590/1980-5373-mr-2016-1089**.
31 M. Rana, C. Banerjee and P. Chowdhury, Studies on optical signal due to oxygen effect on hydrogenated amorphous/crystalline silicon thin films, *Appl. Phys. A: Mater. Sci. Process.*, 2021, **127**, 192, DOI: **10.1007/s00339-021-04322-1**.
32 B. D. Ossonon and D. Bélanger, Synthesis and characterization of sulfophenyl-functionalized reduced graphene oxide sheets, *RSC Adv.*, 2017, **7**, 27224–27234, DOI: **10.1039/C6RA28311J**.
33 N. Majoul, S. Aouida and B. Bessaïs, Progress of porous silicon APTES-functionalization by FTIR investigations, *Appl. Surf. Sci.*, 2015, **331**, 388–391, DOI: **10.1016/j.apsusc.2015.01.107**.
34 T. Oh and C. K. Choi, Comparison between SiOC thin films fabricated by using plasma enhance chemical vapor deposition and SiO2 thin films by using fourier transform infrared spectroscopy, *J. Korean Phys. Soc.*, 2010, **56**, 1150–1155.
35 J. Tinio, K. Simfroso, A. D. M. Opeda and R. Candidato Jr., Influence of OH − Ion Concentration on the Surface Morphology of ZnO-SiO 2 Nanostructure, *J. Nanotechnol.*, 2015, **2015**, 1–7, DOI: **10.1155/2015/686021**.
36 A. Naumann, A novel procedure for strain classification of fungal mycelium by cluster and artificial neural network analysis of Fourier transform infrared (FTIR) spectra, *Analyst*, 2009, **134**, 1215–1223, DOI: **10.1039/B821286D**.
37 M. E. Antinori, L. Ceseracciu, G. Mancini, J. A. Heredia-Guerrero and A. Athanassiou, Fine-Tuning of Physicochemical Properties and Growth Dynamics of Mycelium-Based Materials, *ACS Appl. Bio Mater.*, 2020, **3**, 1044–1051, DOI: **10.1021/acsabm.9b01031**.
38 D. R. Ceratti, *et al.*, Critical effect of pore characteristics on capillary infiltration in mesoporous films, *Nanoscale*, 2015, **7**, 5371–5382, DOI: **10.1039/C4NR03021D**.
39 B. Xu and Q. Zhang, Preparation and Properties of Hydrophobically Modified Nano-SiO2 with Hexadecyltrimethoxysilane, *ACS Omega*, 2021, **6**, 9764–9770, DOI: **10.1021/acsomega.1c00381**.
40 S. Xie, L. Guo, M. Zhang, J. Qin and R. Hu, Durable hydrophobic ceramics of Al2O3–ZrO2 modified by hydrophilic silane with high oil/water separation efficiency, *J. Porous Mater.*, 2021, **28**, 1115–1127, DOI: **10.1007/s10934-021-01055-7**.
41 Y. Yang, *et al.*, Synthesis of Amphiphilic Silica with High Exposure of Surface Groups and Its Utilization in Efficient Removal of Organic Dyes from Aqueous Solution, *Adv. Funct. Mater.*, 2022, **32**, 2106828, DOI: **10.1002/adfm.202106828**.
42 J. Cavalcante and G. Szekely, Surface engineering of a superamphiphilic, self-growing fibrous Janus membrane prepared from mycelium, *J. Mater. Chem. A*, 2023, **11**, 24598–24607, DOI: **10.1039/D3TA05220F**.
43 N. Khan, Z. A. Tabasi, J. Liu, B. H. Zhang and Y. Zhao, Recent Advances in Functional Materials for Wastewater Treatment: From Materials to Technological Innovations, *J. Mar. Sci. Eng.*, 2022, **10**, 534.
44 M. Jones, A. Mautner, S. Luenco, A. Bismarck and S. John, Engineered mycelium composite construction materials from fungal biorefineries: A critical review, *Mater. Des.*, 2020, **187**, 108397, DOI: **10.1016/j.matdes.2019.108397**.
45 M. I. Ojovan and R. F. Tournier, On Structural Rearrangements Near the Glass Transition Temperature in Amorphous Silica, *Materials*, 2021, **14**, 5235, DOI: **10.3390/ma14185235**.
46 T. Wu, *et al.*, Recent Advances in Carbon-Silica Composites: Preparation, Properties, and Applications, *Catalysts*, 2022, **12**(5), 573.
47 M. Haneef, *et al.*, Advanced Materials From Fungal Mycelium: Fabrication and Tuning of Physical Properties, *Sci. Rep.*, 2017, **7**, 41292, DOI: **10.1038/srep41292**.